

Reduction of calcium release site models via moment fitting of phase-type distributions

This article has been downloaded from IOPscience. Please scroll down to see the full text article.

2011 Phys. Biol. 8 026015

(<http://iopscience.iop.org/1478-3975/8/2/026015>)

View [the table of contents for this issue](#), or go to the [journal homepage](#) for more

Download details:

IP Address: 128.239.128.86

The article was downloaded on 07/04/2011 at 16:14

Please note that [terms and conditions apply](#).

Reduction of calcium release site models via moment fitting of phase-type distributions

M Drew LaMar¹, Peter Kemper² and Gregory D Smith¹

¹ Department of Applied Science, The College of William and Mary, Williamsburg, VA 23187, USA

² Department of Computer Science, The College of William and Mary, Williamsburg, VA 23187, USA

E-mail: mdlama@wm.edu

Received 19 October 2010

Accepted for publication 11 March 2011

Published 6 April 2011

Online at stacks.iop.org/PhysBio/8/026015

Abstract

Models of calcium (Ca^{2+}) release sites derived from continuous-time Markov chain (CTMC) models of intracellular Ca^{2+} channels exhibit collective gating reminiscent of the experimentally observed phenomenon of Ca^{2+} puffs and sparks. In order to overcome the state-space explosion that occurs in compositionally defined Ca^{2+} release site models, we have implemented an automated procedure for model reduction that replaces aggregated states of the full release site model with much simpler CTMCs that have similar within-group phase-type sojourn times and inter-group transitions. Error analysis based on comparison of full and reduced models validates the method when applied to release site models composed of 20 three-state channels that are both activated and inactivated by Ca^{2+} . Although inspired by existing techniques for fitting moments of phase-type distributions, the automated reduction method for compositional Ca^{2+} release site models is unique in several respects and novel in this biophysical context.

1. Introduction

Cell signal transduction is often mediated by molecular assemblies composed of multiple interacting transmembrane receptors [1, 2]. For example, in coliform bacteria, the high sensitivity of lattices of plasma membrane proteins to chemoattractants is due to allosteric protein–protein interactions leading to conformational spread through the receptor array [3]. In rat basophilic leukemia (RBL) cells, cross-linking of immunoglobulin E receptors (FcεR1) with multivalent antigen leads to tyrosine kinase-dependent activation of phospholipase C_γ , production of inositol 1,4,5-trisphosphate (IP_3), release of Ca^{2+} from intracellular stores, clustering of IP_3 receptor Ca^{2+} channels (IP_3Rs), sustained Ca^{2+} influx, and secretion of histamine and other mediators of inflammation [4, 5]. Systems biologists seek principles that govern the emergent behavior of signaling complexes and a robust conceptual framework for biological modeling of these molecular assemblies.

Signaling complexes are not restricted to the plasma membrane (PM), but are also found on mitochondrial

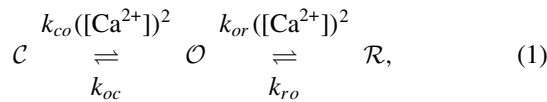
and nuclear membranes and on the endoplasmic (ER) or sarcoplasmic (SR) reticulum [6–8]. Clusters of 5–50 IP_3Rs on both the cortical ER [9, 10] and outer nuclear membrane [11] of immature *Xenopus laevis* oocytes exhibit coordinated gating that gives rise to spatially localized Ca^{2+} elevations known as ‘ Ca^{2+} puffs.’ During cardiac excitation–contraction coupling, PM depolarization leads to Ca^{2+} influx via L-type Ca^{2+} channels that triggers ‘ Ca^{2+} sparks,’ i.e. the release of SR Ca^{2+} from two-dimensional arrays of ryanodine receptors (RyRs).

While there is consensus that Ca^{2+} regulation of IP_3Rs and RyRs, multiple cytoplasmic and luminal accessory proteins, and allosteric protein–protein interactions generate the concerted activity of Ca^{2+} release sites [12–14], the biophysical theory relating single channel kinetics of intracellular Ca^{2+} channels to the emergent dynamics of Ca^{2+} puffs and sparks is in development [15–22]. Ca^{2+} signaling complexes can be idealized as stochastic automata networks (SANs) that involve many functional transitions whose rates depend on the state of other channels in the release site [16]. This promising theoretical perspective combines Markov

chain modeling of the stochastic gating of intracellular Ca^{2+} channels with an idealized representation of the coupling of channels via allosteric interactions and/or localized elevations in intracellular Ca^{2+} . However, the compositional nature of Ca^{2+} signaling complexes and the resulting combinatorial state-space explosion leads to significant challenges for the analysis and reduction of SAN models [23, 24]. This paper focuses on the automated reduction of compositionally defined Ca^{2+} signaling complexes, an important step toward mechanistic modeling of Ca^{2+} dynamics that traverses the molecular and cellular levels of biological organization.

1.1. Markov chain models of single channel gating

The stochastic gating of voltage- and ligand-gated ion channels—experimentally observed using single channel recording techniques—is often modeled using discrete-state continuous-time Markov chains (CTMCs) [25–27]. The topology of Markov chain models of single channel gating can be summarized by a diagram that indicates the possible states a channel may occupy and allowed transitions between these states. For example, the state–transition diagram for a minimal model of a Ca^{2+} -regulated intracellular Ca^{2+} channel,



includes one open state \mathcal{O} and two closed states: a short-lived closed state \mathcal{C} and a long-lived closed (i.e. refractory) state \mathcal{R} . The $\mathcal{C} \rightarrow \mathcal{O}$ and $\mathcal{O} \rightarrow \mathcal{R}$ transitions correspond to Ca^{2+} -mediated activation and inactivation of the channel, respectively. In this state–transition diagram, $k_{co}([\text{Ca}^{2+}]^2)$, k_{oc} , $k_{or}([\text{Ca}^{2+}]^2)$, and k_{ro} are transition rates with units of time^{-1} , k_{co} and k_{or} are association rate constants with units of $\text{conc}^{-2} \text{time}^{-1}$, and $[\text{Ca}^{2+}]$ is the local concentration of intracellular Ca^{2+} experienced by the channel. For simplicity, this model does not explicitly account for the homotetrameric structure of individual IP_3Rs and RyRs and it is assumed that the cooperativity of Ca^{2+} binding is the same for the activation and inactivation processes.

While models for intracellular Ca^{2+} channels such as the IP_3R and the RyR can be significantly more complicated [28–30], they often can be written in the form

$$Q([\text{Ca}^{2+}]) = K_- + ([\text{Ca}^{2+}])^\eta K_+, \quad (2)$$

where K_+ is a square matrix of bimolecular (Ca^{2+} -dependent) transition rates, and K_- collects the unimolecular, Ca^{2+} -independent transition rates [16]. For example, the K_- and K_+ matrices corresponding to the three-state model in (1) are

$$K_+ = \begin{pmatrix} -k_{co} & k_{co} & 0 \\ 0 & -k_{or} & k_{or} \\ 0 & 0 & 0 \end{pmatrix}$$

and

$$K_- = \begin{pmatrix} 0 & 0 & 0 \\ k_{oc} & -k_{oc} & 0 \\ 0 & k_{ro} & -k_{ro} \end{pmatrix},$$

where the rows and columns of each matrix correspond to the states \mathcal{C} , \mathcal{O} , and \mathcal{R} (in that order). Because the cooperativity of

Ca^{2+} binding is $\eta = 2$ in (1), the Q -matrix for the three-state channel in (2) is

$$Q(c) = \begin{pmatrix} -k_{co}([\text{Ca}^{2+}]^2) & k_{co}([\text{Ca}^{2+}]^2) & 0 \\ k_{oc} & -k_{oc} - k_{or}([\text{Ca}^{2+}]^2) & k_{or}([\text{Ca}^{2+}]^2) \\ 0 & k_{ro} & -k_{ro} \end{pmatrix}. \quad (3)$$

In the general case, the matrix $Q = (q_{ij})$ is referred to as the infinitesimal generator matrix (or Q -matrix) for the CTMC $X(t)$ that takes integer values between 1 and M (the number of states). The off-diagonal elements of Q give the probability per unit time of a transition from state i to state j ,

$$q_{ij} = \lim_{\delta t \rightarrow 0} P\{X(t + \delta t) = j | X(t) = i\} / \delta t \quad (i \neq j), \quad (4)$$

while the absolute value of the diagonal elements correspond to the probability per unit time of a transition out of each state,

$$|q_{ii}| = \lim_{\delta t \rightarrow 0} P\{X(t + \delta t) \neq i | X(t) = i\} / \delta t. \quad (5)$$

If we write the probability distribution over channel states as a row vector, e.g., $\pi(t) = (\pi_{\mathcal{C}}, \pi_{\mathcal{O}}, \pi_{\mathcal{R}})$, then the time evolution of this distribution can be found by solving the ordinary differential equation system

$$\frac{d\pi}{dt} = \pi Q, \quad (6)$$

where $\pi(0)$ is an initial distribution satisfying $\sum_i \pi_i = 1$, that is, $\pi e = 1$ where e is a commensurate column vector of ones. Equations (4) and (5) imply that the diagonal entries of Q are the opposite of the sum of the off-diagonal entries in the same row, that is, $q_{ii} = -\sum_{j \neq i} q_{ij}$ (cf (3)). This condition ensures conservation of probability, as can be seen by multiplying (6) on the right by e to give $d(\pi e)/dt = \pi Q e = 0$. For further review of Markov chains from a mathematical perspective see [31].

Markov chain models of single channel gating have a finite number of states and are irreducible, that is, it is possible to move between any two states via one or more transitions. The limiting probability distribution of such Markov chains (found by integrating (6) for a long time) does not depend on the initial condition $\pi(0)$ and is equal to the unique stationary distribution $\bar{\pi}$ satisfying

$$\bar{\pi} Q = 0 \quad \text{subject to} \quad \bar{\pi} e = 1. \quad (7)$$

For review of numerical methods for calculating the stationary distribution of Markov chains see [32].

For the three-state model in (1), an analytical expression for the stationary distribution is easily found. In particular, the open probability for this single channel model is

$$\pi_{\mathcal{O}} = \frac{([\text{Ca}^{2+}])^2 K_{\text{inact}}}{K_{\text{act}} K_{\text{inact}} + ([\text{Ca}^{2+}])^2 K_{\text{inact}} + ([\text{Ca}^{2+}])^4},$$

where $K_{\text{act}} = \sqrt{k_{oc}/k_{co}}$ and $K_{\text{inact}} = \sqrt{k_{ro}/k_{or}}$ are dissociation constants for Ca^{2+} activation and inactivation, respectively. The standard parameter values of $K_{\text{act}} = 0.58 \mu\text{M}$ and $K_{\text{inact}} = 0.76 \mu\text{M}$ result in a single channel open probability that is a bell-shaped function of $[\text{Ca}^{2+}]$, consistent with experimental observations of intracellular Ca^{2+} channels such as the IP_3R and the RyR .

1.2. Compositional Ca^{2+} release site models

Clustered IP₃R and RyR participate in forming a dynamic Ca^{2+} microdomain that influences the local $[Ca^{2+}]$ experienced by each channel [33, 34]. Assuming that the dwell times of channel states are long compared to the time scale of local $[Ca^{2+}]$ changes, the microdomain $[Ca^{2+}]$ profile can be calculated from the position and source amplitude of open channels using well-known equations for the buffered diffusion of Ca^{2+} [35, 36]. The coupling of Ca^{2+} -regulated channels that are distinguishable due to their spatial location can lead to release site models with large state spaces. For example, a release site composed of 20 instantaneously coupled three-state channels has $3^{20} \approx 3.5 \times 10^9$ states. Due to this combinatorial state-space explosion, Ca^{2+} release site models are often constructed under the assumption of mean-field coupling [16, 37]. In the simplest case, each channel is assumed to experience a domain $[Ca^{2+}]$ that is an algebraic function of the number of open channels at the release site, for example,

$$[Ca^{2+}](t) = \begin{cases} c_{\infty} + c_* N_{\mathcal{O}}(t), & \text{when channel closed,} \\ c_{\infty} + c_*(N_{\mathcal{O}}(t) - 1) + c_d, & \text{when channel open,} \end{cases} \quad (8)$$

where c_{∞} is the background cytosolic $[Ca^{2+}]$, c_* is the coupling strength and c_d is the substantially elevated $[Ca^{2+}]$ that the channel experiences when open. Prior work has investigated the validity of various mean-field formulations for allosteric channel interactions and those mediated through elevated local $[Ca^{2+}]$ [17, 38]. For the purposes of this paper it is sufficient to restrict attention to channels coupled via (8).

In general, a release site composed of N identical and indistinguishable M -state channels has

$$\beta(N, M) = \binom{M + N - 1}{N}$$

states. More concretely, a release site composed of N identical mean-field coupled three-state channels (see (1)) has $\beta(N, 3) = (N + 2)(N + 1)/2$ distinct states that may be enumerated anti-lexicographically as

$$(N, 0, 0), (N - 1, 1, 0), \dots, (0, 1, N - 1), (0, 0, N), \quad (9)$$

where each configuration takes the form $(N_C, N_{\mathcal{O}}, N_{\mathcal{R}})$ with $0 \leq N_C \leq N$, $0 \leq N_{\mathcal{O}} \leq N$, $0 \leq N_{\mathcal{R}} \leq N$, and $N_C + N_{\mathcal{O}} + N_{\mathcal{R}} = N$. When these N channels are coupled via (8), the nonnegative elements of an expanded generator matrix for this release site are

$$Q[(N_C, N_{\mathcal{O}}, N_{\mathcal{R}}), (N_C - 1, N_{\mathcal{O}} + 1, N_{\mathcal{R}})]$$

$$= N_C k_{co} (c_{\infty} + N_{\mathcal{O}} c_*)^2$$

$$Q[(N_C, N_{\mathcal{O}}, N_{\mathcal{R}}), (N_C + 1, N_{\mathcal{O}} - 1, N_{\mathcal{R}})] = N_{\mathcal{O}} k_{oc}$$

$$Q[(N_C, N_{\mathcal{O}}, N_{\mathcal{R}}), (N_C, N_{\mathcal{O}} - 1, N_{\mathcal{R}} + 1)]$$

$$= N_{\mathcal{O}} k_{or} (c_{\infty} + (N_{\mathcal{O}} - 1) c_* + c_d)^2$$

$$Q[(N_C, N_{\mathcal{O}}, N_{\mathcal{R}}), (N_C, N_{\mathcal{O}} + 1, N_{\mathcal{R}} - 1)] = N_{\mathcal{R}} k_{ro},$$

where it is understood that the origin and destination configurations of the release site must both be valid (i.e. must

both occur in (9)). In the case of $N = 20$ three-state channels, there are $\beta(20, 3) = 231$ distinguishable release site states. Figure 1 shows two representative release site simulations with 20 three-state channels exhibiting stochastic excitability that is reminiscent of Ca^{2+} puffs and sparks.

IP₃R and RyR models can be significantly more complicated than the three-state model in (1); when composed of multiple subunits they may involve tens or even hundreds of states [28–30]. Because physiologically realistic values for N are in the range 20–200, and $\beta(N, M)$ is on the order of N^{M-1} , even these ‘minimal’ release site models that assume mean-field coupling may have extremely large state spaces.

1.3. Automated reduction of Ca^{2+} release site models

This paper presents a novel approach to the automated reduction of Ca^{2+} release site models that are composed of stochastically gating channels as in section 1.2. The complexity of a release site model is not a significant concern when Monte Carlo simulation techniques are used to simulate the stochastic dynamics of individual Ca^{2+} release events. However, multiscale whole cell simulations that include both local and global Ca^{2+} signals require release site models that are as compact as possible while retaining the physiological realism of interacting channels and collective gating [40–44]. Indeed, for computational modeling to contribute to mechanistic understanding of the cellular effect of pharmacological manipulations of single channel gating, a Ca^{2+} release site model must be compositional. In addition, direct calculation of release site properties (e.g., mean puff/spark duration) is most efficiently performed using matrix analytic expressions that scale with the number of release site states. Consequently, development of methods for the automated reduction of compositional Ca^{2+} release site models (e.g., application of lumpability results for structured Markov chains [45–47]) is an important research objective.

In prior work we have investigated the automated reduction of Ca^{2+} release site models that begins with categorization of the single channel model rate constants as either fast or slow [24]. Groups of states connected by fast transitions are aggregated and transition rates between reduced states are chosen consistent with the conditional probability distribution among states within each group. For small test problems, these conditional probability distributions can be calculated from the full model without approximation. For the larger problems, the conditional probability distributions can be approximated without the construction of the full model by assuming rapid mixing of states connected by fast transitions; alternatively, memory-efficient iterative aggregation/disaggregation may be employed [48, 49].

Fast–slow reductions, however, may not preserve the group structure corresponding to the number of open channels (as seen in [24], for example), which is an important quantity for comparison with experimental observables [50] as well as insertion into multiscale models of whole cell response (via (8)). There exist other techniques for model simplification,

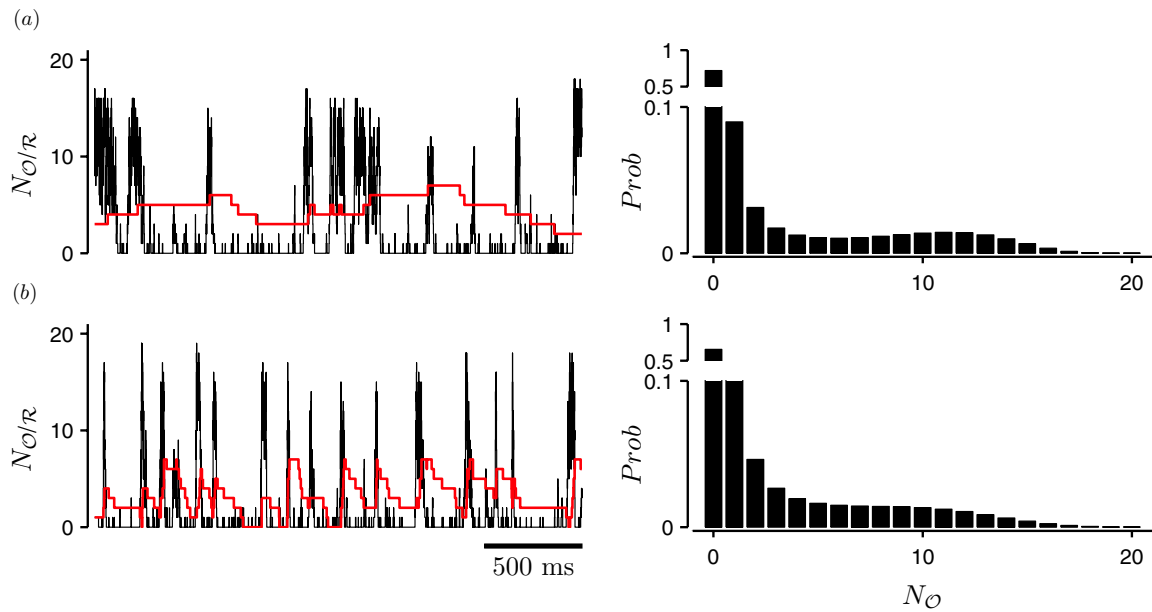


Figure 1. (a) Release site simulation with 20 three-state channels exhibiting stochastic excitability reminiscent of Ca^{2+} puffs and sparks. Left: the number of open (N_O , black line) and inactivated (N_R , red line) channels as a function of time. Because the dynamics of Ca^{2+} inactivation and de-inactivation are relatively slow, puff/spark termination occurs via a process of stochastic attrition (see [39] for further discussion). Right: stationary probability distribution for the number of open channels (N_O). Parameters: $c_\infty = 0.05 \mu\text{M}$, $c_* = 0.075 \mu\text{M}$, $c_d = 0.5 \mu\text{M}$, $k_{co} = 1.5 \mu\text{M}^{-2} \text{ms}^{-1}$, $k_{oc} = 0.5 \text{ms}^{-1}$, $K_{\text{act}} = \sqrt{k_{oc}/k_{co}} = 0.58 \mu\text{M}$; $k_{or} = 0.0015 \mu\text{M}^{-2} \text{ms}^{-1}$, $k_{ro} = 0.00087 \text{ms}^{-1}$, $K_{\text{inact}} = \sqrt{k_{ro}/k_{or}} = 0.76 \mu\text{M}$. (b) Ca^{2+} release site simulation in which the dynamics of Ca^{2+} inactivation and de-inactivation are 10-fold faster. In this case puffs terminate via the recruitment of inactivated channels. Parameters as in (a) save $k_{or} = 0.015 \mu\text{M}^{-2} \text{ms}^{-1}$ and $k_{ro} = 0.0087 \text{ms}^{-1}$; K_{act} and K_{inact} remain unchanged.

for example invariant manifold reduction [51, 52]. In these references, single channel models as well as collections of independent channels or subunits have solutions consisting of parametrized distributions, where the parameters satisfy a much smaller system of differential equations than the original master equation. While exploration in this direction with our compositionally defined release sites is of interest, it is currently not useful in our whole-cell context since our channels are coupled in a non-trivial manner.

In contrast to fast–slow reductions, this paper introduces a technique for automated Ca^{2+} release site reduction that does not require a separation of time scales. While inspired by approximate constructions such as Markov arrival processes [53], the method is unique in several respects and novel in this biophysical context. As presented in section 2, reduction is achieved by replacing aggregated states of the full release site model with much simpler CTMCs that have similar phase-type sojourn times between inter-group transitions. Section 3 validates the method when applied to release site models composed of 20 three-state channels (see sections 1.1 and 1.2). Section 4 discusses generalizations of this approach to automated Ca^{2+} release site reduction and suggestions for further research.

2. Automated Ca^{2+} release site model reduction

The automated reduction method that is the focus of this paper can be applied to release site models of arbitrary size and complexity, and we therefore illustrate the approach in

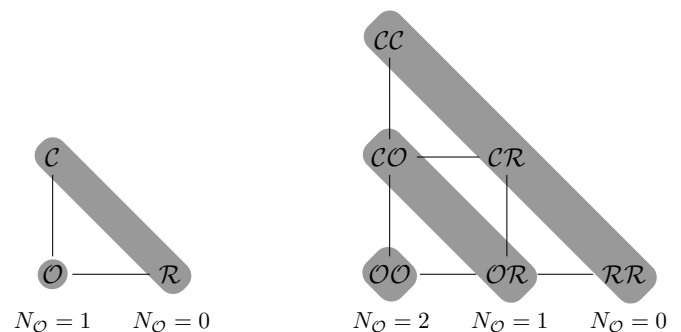


Figure 2. Left: three-state single channel model in (1). Shaded regions partition states into two groups based on the number of open channels ($N_O = 0, 1$). Right: partitioning a release site model composed of two mean-field coupled three-state models leads to three groups of sizes 1, 2, and 3.

full generality using release sites composed of N arbitrary yet identical channels. We will, however, refer to the three-state model in (1) as needed for clarification and validation.

The method begins by partitioning the model state space into $N + 1$ groups ($\mathcal{P}_0, \mathcal{P}_1, \dots, \mathcal{P}_N$) where \mathcal{P}_i includes all release site states with i open channels ($N_O = i$, see figure 2). This partitioning strategy is consistent with our primary interest in the stochastic dynamics of the number of open channels and the local $[\text{Ca}^{2+}]$ (the experimental observable). The Q -matrix is permuted into the following

For example, if we construct the reduced model so that the probability distribution of the sojourn time in each block is given by a *two-state hyper-exponential distribution*, $PH(\hat{\alpha}, \hat{T})$, then using the constraints that $\hat{\alpha}e = 1$ and $\hat{u} = -\hat{T}e$ we have

$$\hat{\alpha} = (\hat{\alpha} \quad 1 - \hat{\alpha}), \quad \hat{T} = \begin{pmatrix} -\hat{u}_1 & 0 \\ 0 & -\hat{u}_2 \end{pmatrix}, \quad \hat{u} = \begin{pmatrix} \hat{u}_1 \\ \hat{u}_2 \end{pmatrix}, \quad (17)$$

with *three* scalar parameters to be determined: $\hat{u}_1 > 0$, $\hat{u}_2 > 0$, and $0 < \hat{\alpha} < 1$. Using (16) and elementary properties of diagonal matrices, the moments of a two-state hyper-exponential distribution are

$$\begin{aligned} \hat{m}_k &= k!(\hat{\alpha} \quad 1 - \hat{\alpha}) \begin{pmatrix} \hat{u}_1 & 0 \\ 0 & \hat{u}_2 \end{pmatrix}^{-k} \begin{pmatrix} 1 \\ 1 \end{pmatrix} \\ &= k! \left[\frac{\hat{\alpha}}{\hat{u}_1^k} + \frac{1 - \hat{\alpha}}{\hat{u}_2^k} \right]. \end{aligned} \quad (18)$$

Setting the first and second moments ($k = 1, 2$) of this expression equal to the first and second moments of the phase-type distributions of the full model, simultaneously for both $PH(\hat{\alpha}^-, \hat{T})$ and $PH(\hat{\alpha}^+, \hat{T})$, leads to the following four equations:

$$\begin{aligned} m_1^\pm &= \frac{\hat{\alpha}^\pm}{\hat{u}_1} + \frac{1 - \hat{\alpha}^\pm}{\hat{u}_2} \\ m_2^\pm &= 2 \left(\frac{\hat{\alpha}^\pm}{\hat{u}_1^2} + \frac{1 - \hat{\alpha}^\pm}{\hat{u}_2^2} \right), \end{aligned}$$

with four unknowns: $\hat{\alpha}^-$, $\hat{\alpha}^+$, \hat{u}_1 , and \hat{u}_2 . These equations can be rewritten as

$$m_1^\pm \hat{u}_1 \hat{u}_2 = \hat{\alpha}^\pm (\hat{u}_2 - \hat{u}_1) + \hat{u}_1 \quad (19)$$

$$m_2^\pm \hat{u}_1^2 \hat{u}_2^2 = 2\hat{\alpha}^\pm (\hat{u}_2^2 - \hat{u}_1^2) + 2\hat{u}_1^2. \quad (20)$$

Substituting $\hat{\alpha}^\pm (\hat{u}_2 - \hat{u}_1) = m_1^\pm \hat{u}_1 \hat{u}_2 - \hat{u}_1$ from (19) into (20) gives

$$m_2^\pm \hat{u}_1 \hat{u}_2 = 2m_1^\pm (\hat{u}_1 + \hat{u}_2) - 2.$$

Writing the unknowns as $x = \hat{u}_1 + \hat{u}_2$ and $y = \hat{u}_1 \hat{u}_2$, we find that choosing the reduced model parameters requires finding x and y that minimize

$$\left\| \begin{pmatrix} 2m_1^- & -m_2^- \\ 2m_1^+ & -m_2^+ \end{pmatrix} \begin{pmatrix} x \\ y \end{pmatrix} - \begin{pmatrix} 2 \\ 2 \end{pmatrix} \right\|_2 \quad (21)$$

subject to inequality constraints $0 < \hat{\alpha}^\pm < 1$, $x, y > 0$ and $x^2 > 4y$ where

$$\hat{\alpha}^\pm = \frac{\hat{u}_1 (m_1^\pm \hat{u}_2 - 1)}{\hat{u}_2 - \hat{u}_1} \quad \text{and} \quad \hat{u}_{1/2} = \frac{x \pm \sqrt{x^2 - 4y}}{2}.$$

Next, we use the zeroth moment ($k = 0$) to split the exit rate vector \hat{u} into two components, \hat{u}^- and \hat{u}^+ . The joint moments for phase-type distributions with two exit rate vectors, $PH(\alpha^\pm, T, \mathbf{u}^\pm)$, are

$$m_k^{\pm, \pm} = k! \alpha^\pm (-T)^{-(k+1)} \mathbf{u}^\pm,$$

where $\alpha^\pm e = 1$, $\mathbf{u}^- + \mathbf{u}^+ = -Te$. Thus, the four target moments from the homogenized full model are

$$m_0^{\pm, \pm} = \alpha^\pm (-T)^{-1} \mathbf{u}^\pm. \quad (22)$$

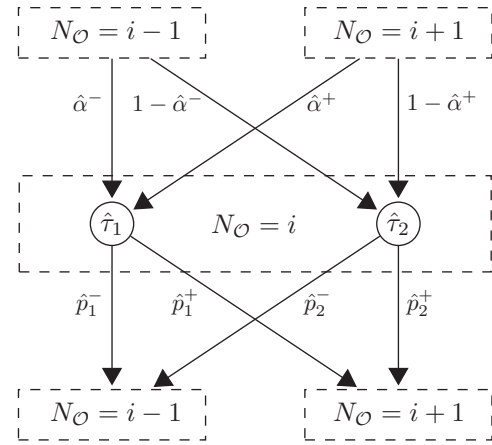


Figure 4. Diagrammatic representation of the dynamics of the two-state hyper-exponential phase-type distributions $PH(\hat{\alpha}^\pm, \hat{T}, \hat{u}^\pm)$ of the reduced model when $N_O = i$. The probability distributions $(\hat{\alpha}^-, 1 - \hat{\alpha}^-)$ and $(\hat{\alpha}^+, 1 - \hat{\alpha}^+)$ give the probabilities for entering two substates with mean dwell times of $\hat{\tau}_1$ and $\hat{\tau}_2$, given that you arrived from states $N_O = i - 1$ and $i + 1$, respectively. The probabilities \hat{p}_1^\pm and \hat{p}_2^\pm are the probabilities of proceeding to states $N_O = i - 1$ and $i + 1$ from each substate (see (25)).

The corresponding moments of the two-state hyper-exponential distributions of the reduced model can be written as

$$\begin{aligned} \begin{pmatrix} \hat{m}_0^{-, -} & \hat{m}_0^{-, +} \\ \hat{m}_0^{+, -} & \hat{m}_0^{+, +} \end{pmatrix} &= \begin{pmatrix} \hat{\alpha}^- & 1 - \hat{\alpha}^- \\ \hat{\alpha}^+ & 1 - \hat{\alpha}^+ \end{pmatrix} \\ &\times \begin{pmatrix} \hat{u}_1 & 0 \\ 0 & \hat{u}_2 \end{pmatrix}^{-1} \begin{pmatrix} \hat{u}_1^- & \hat{u}_1^+ \\ \hat{u}_2^- & \hat{u}_2^+ \end{pmatrix}, \end{aligned} \quad (23)$$

where $\hat{u}_1 = \hat{u}_1^- + \hat{u}_1^+$ and $\hat{u}_2 = \hat{u}_2^- + \hat{u}_2^+$. The latter two equations imply we have two free parameters and thus we only use the two equations corresponding to the first column in (23). The final step in moment fitting is thus to find the values of \hat{u}_1^- and \hat{u}_2^- that minimize

$$\left\| \begin{pmatrix} m_0^{-, -} \\ m_0^{+, -} \end{pmatrix} - \begin{pmatrix} \hat{\alpha}^- / \hat{u}_1 & (1 - \hat{\alpha}^-) / \hat{u}_2 \\ \hat{\alpha}^+ / \hat{u}_1 & (1 - \hat{\alpha}^+) / \hat{u}_2 \end{pmatrix} \begin{pmatrix} \hat{u}_1^- \\ \hat{u}_2^- \end{pmatrix} \right\|_2 \quad (24)$$

subject to the constraints $0 < \hat{u}_1^- < \hat{u}_1$ and $0 < \hat{u}_2^- < \hat{u}_2$.

The minimizations necessary for moment fitting in (21) and (24) can often be attained by solving the corresponding linear algebraic systems. If this solution does not satisfy the inequality constraints, minimization can be performed using an appropriate optimization routine (e.g. linear least-squares in (24)). The moment fitting scheme employed for the interior blocks T_i for $1 \leq i \leq N - 1$ are modified when $i = 0$ or N (see the appendix) as there is only one way to enter and leave the blocks in these special cases.

2.5. Diagrammatic representation of the dynamics of the reduced model

Figure 4 shows a diagrammatic representation of the hyper-exponential distributions in the reduced model. The transient matrix \hat{T}_i corresponding to $N_O = i$ open channels has two nonzero elements, \hat{u}_1 and \hat{u}_2 (the index i is dropped for clarity),

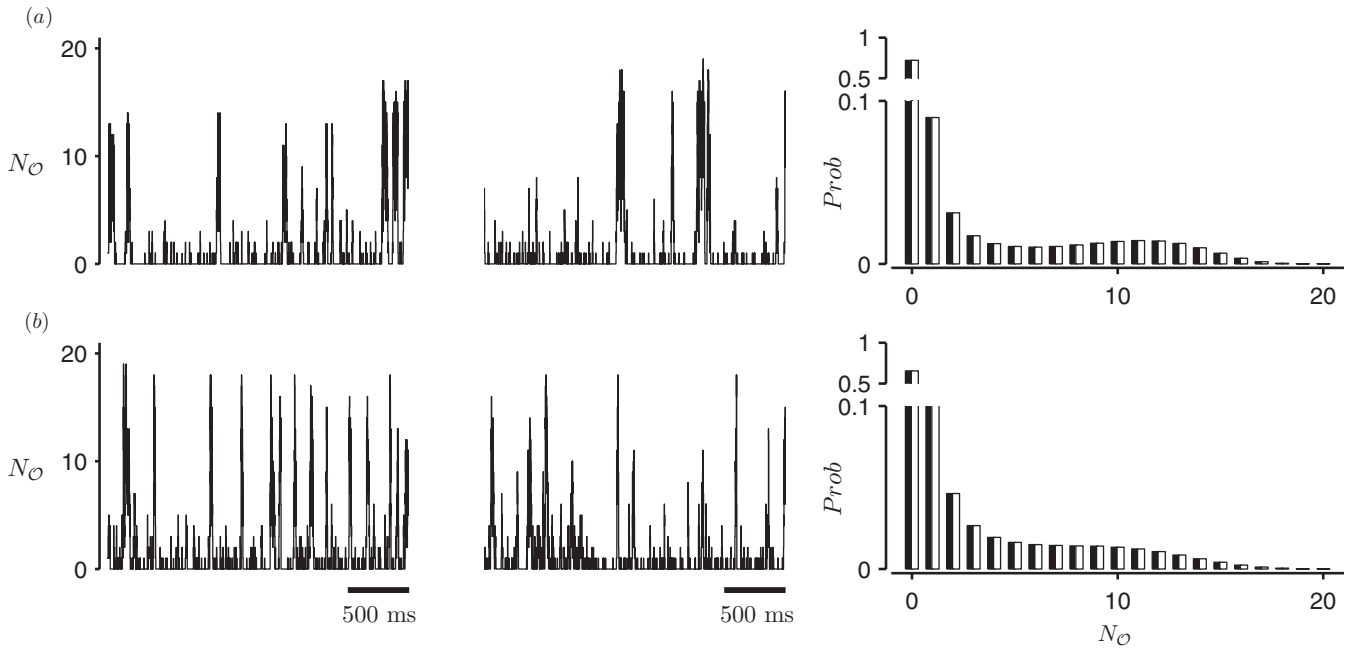


Figure 5. (a) Full and reduced Ca^{2+} release site simulations with 20 three-state channels (left and middle plots, respectively). Parameters as in figure 1(a). The right plot compares the steady state distribution for the number of open channels (N_O) for the full and reduced models (black and white bars, respectively). (b) Similar results obtained using the parameters in figure 1(b).

with dwell times given by $\hat{\tau}_1 = 1/\hat{u}_1$ and $\hat{\tau}_2 = 1/\hat{u}_2$. If the i th block is entered from below ($i - 1$), the substate with mean dwell time $\hat{\tau}_1$ and $\hat{\tau}_2$ is entered with probability $\hat{\alpha}^-$ and $1 - \hat{\alpha}^-$, respectively. If the i th block is entered from above ($i + 1$), these substates are entered with probabilities $\hat{\alpha}^+$ and $1 - \hat{\alpha}^+$.

The exit rate vectors \hat{u}_i^\pm associated with the i th block determine if the subsequent block has $N_O = i - 1$ or $i + 1$ open channels. Upon entry into the $\hat{\tau}_1$ substate of the i th block, the probabilities of a decreasing or increasing number of open channels are

$$\hat{p}_1^- = \frac{\hat{u}_1^-}{\hat{u}_1^- + \hat{u}_1^+} \quad \text{and} \quad \hat{p}_1^+ = 1 - \hat{p}_1^- = \frac{\hat{u}_1^+}{\hat{u}_1^- + \hat{u}_1^+}, \quad (25)$$

where again we drop the index i for clarity. Similarly, entry of the $\hat{\tau}_2$ substate results in a decreasing or increasing number of open channels with probabilities $\hat{p}_2^- = \hat{u}_2^- / (\hat{u}_2^- + \hat{u}_2^+)$ and $\hat{p}_2^+ = 1 - \hat{p}_2^- = \hat{u}_2^+ / (\hat{u}_2^- + \hat{u}_2^+)$.

3. Validation of the Ca^{2+} release site reduction method

The validation of the Ca^{2+} release site reduction method described in the previous section was performed by comparing the dynamics of full models composed of $N = 20$ mean-field coupled three-state channels in (1) leading to release sites with 231 total states. The reduced model consists of $N + 1 = 21$ diagonal blocks (T_i), 20 of which are two-state hyper-exponential distributions ($N_O = 0, \dots, 19$). Because the $N_O = 20$ partition has only one state in the full model, no reduction is required for the T_N block. The reduced model has $2 \times 20 + 1 = 41$ states, which is an 82% reduction in size compared to the full model ($41/231 \approx 0.18$).

Figure 5 shows the number of open channels $N_O(t)$ over time for model Ca^{2+} release sites composed of 20 three-state channels. Simulations of the 231-state full model and the 41-state reduced model are presented in the left and middle panels, respectively. The right panels show good agreement between the steady state distributions of N_O in the full and reduced models (black and white bars). The parameters used in figures 5(a) and (b) correspond to the two possible roles of Ca^{2+} inactivation in the dynamics of Ca^{2+} spark termination (cf figure 1) [17]. The reduced model reproduces the distribution of N_O in the full model when (a) spark termination occurs through the process of stochastic attrition on a relatively constant background of refractory channels, and also (b) when spark termination occurs via recruitment of refractory channels during each event.

Figure 6 shows a scatter plot of Ca^{2+} event amplitude and duration for simulations of both the full and reduced models. Sparks initiate with an $N_O = 0 \rightarrow 1$ transition at time t_{init} and terminate upon the first subsequent $N_O = 1 \rightarrow 0$ transition at time t_{term} . Spark *duration* = $t_{\text{term}} - t_{\text{init}}$ and spark *amplitude* is the integral of the number of open channels between these times. The marginal distributions of spark duration and amplitude show general agreement between the full and reduced models (black and white bars). Comparison of figures 6(a) and (b) shows that the reduced model captures the dynamics of Ca^{2+} sparks more accurately when spark termination is via stochastic attrition (a) and slightly less accurately when spark termination is due to the accumulation of refractory channels (b).

In order to accurately quantify the error that results from model reduction, we define the error measure $E_{\text{max}}(t) =$

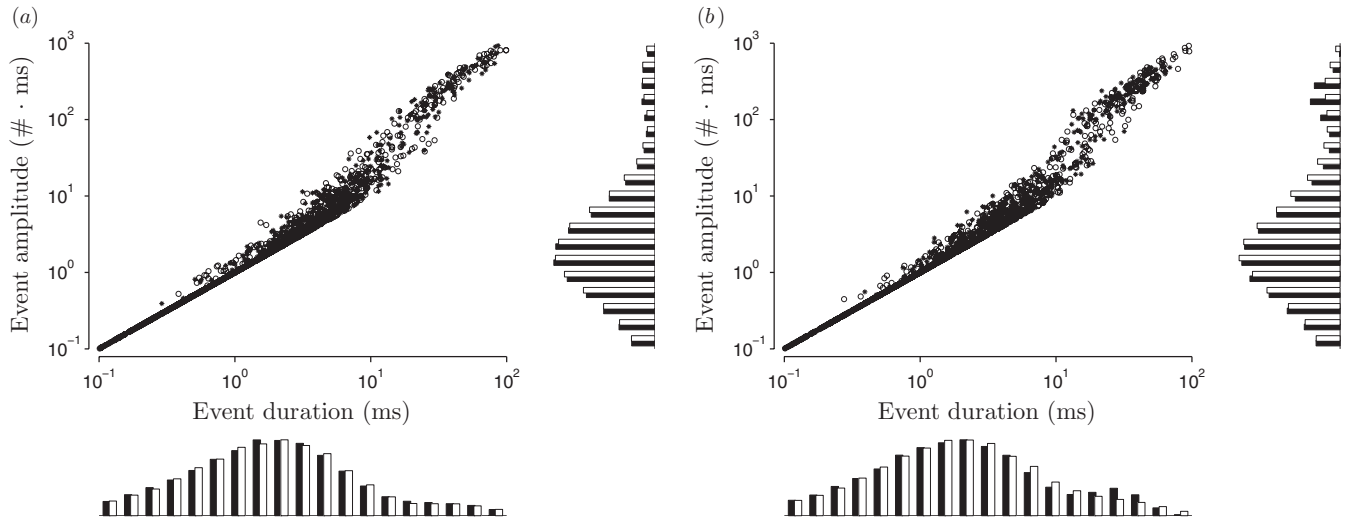


Figure 6. Scatter plots and marginal distributions for Ca^{2+} spark amplitude and duration in simulations of the full and reduced models. Asterisks and black bars denote full model; open circles and white bars denote the reduced model. Parameters as in figure 5.

$\max_{ij} |E_{ij}(t)|$ where $E(t)$ compares the dynamics of $N_{\mathcal{O}}(t)$ in the full and reduced models as follows:

$$E(t) = U \exp(tQ)V - \hat{U} \exp(t\hat{Q})\hat{V}, \quad (26)$$

where Q and \hat{Q} are the generator matrices for the full and reduced models that have $\beta = 231$ and $\hat{\beta} = 41$ states, respectively. In this expression, V is a $\beta \times N + 1$ collector matrix,

$$V = \begin{pmatrix} e_0 & 0 & \cdots & 0 \\ 0 & e_1 & \cdots & 0 \\ \vdots & \vdots & \ddots & \vdots \\ 0 & 0 & \cdots & e_N \end{pmatrix},$$

where $N = 20$ is the number of channels in the release site model, and each e_i is a column vector of ones commensurate with $Q_{i,i}$ (see (10)). The $(N + 1) \times \beta$ distributor matrix U is given by

$$U = \begin{pmatrix} \bar{\pi}_0 & 0 & \cdots & 0 \\ 0 & \bar{\pi}_1 & \cdots & 0 \\ \vdots & \vdots & \ddots & \vdots \\ 0 & 0 & \cdots & \bar{\pi}_N \end{pmatrix},$$

where the row vector $\bar{\pi} = (\bar{\pi}_0 \bar{\pi}_1 \cdots \bar{\pi}_N)$ is the stationary probability distribution of the full model (see (7)). The $\hat{\beta} \times N + 1$ collector (\hat{V}) and $(N + 1) \times \hat{\beta}$ distributor (\hat{U}) matrices for the reduced model are similarly defined.

The solid lines of figures 7(a) and (b) show the error between the full and reduced models ($E_{\max}(t)$) calculated using (26) for the two different release site parameter sets discussed above. In both cases, the error is initially ($t = 0$) and ultimately ($t \rightarrow \infty$) very small ($< 10^{-7}$), but grows modestly to 0.0059 ($t = 74$ ms) in the case of stochastic attrition (a) and 0.041 ($t = 29$ ms) when recruitment of refractory channels terminates sparks (b). The broken lines in figure 7 show the error between the homogenized full model and the reduced model calculated using (26) with the replacement of \hat{Q} for Q . The small size of this error ($< 10^{-3}$ for all t) indicates that the

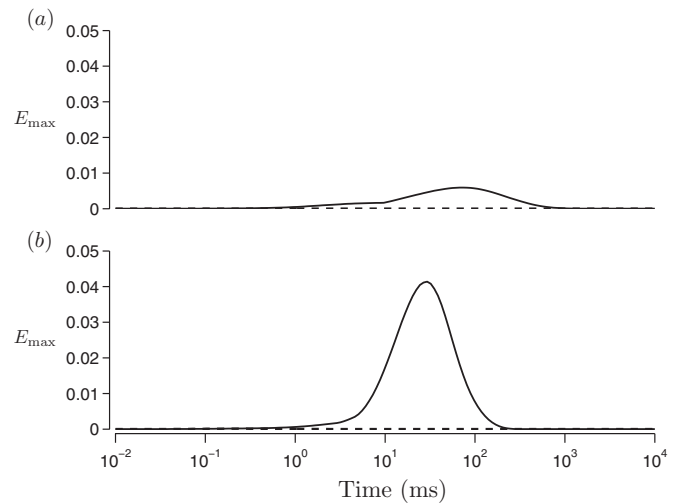


Figure 7. Error of the dynamics of $N_{\mathcal{O}}(t)$ in the reduced model as compared to the full model (see (26), solid lines). This error is dominated by the homogenization of the full model defined in (15) as opposed to inaccuracies in moment fitting (dashed line). Parameters as in figures 1(a) and (b).

reduction error is primarily attributable to the homogenization of the full model in (15) as opposed to the moment fitting procedure *per se* (section 2.4).

4. Discussion

We have described a novel reduction technique applicable to Markov chain models of Ca^{2+} release sites composed of instantaneously mean-field coupled intracellular Ca^{2+} channels. Using 20 three-state channels that are both activated and inactivated by Ca^{2+} , the full and reduced models have nearly identical stationary distributions for the number of open channels (figure 5). The dynamics of $N_{\mathcal{O}}(t)$ and the distribution of spark durations and amplitudes (figure 6) are

also quite similar in considering the 82% reduction in model size obtained.

The Ca^{2+} release site model reduction procedure introduced in this paper includes three major steps: choosing a partitioning scheme that determines how full model states are aggregated (figure 2 and (10)), calculation of target moments using the homogenized full model (sections 2.2 and 2.3), and moment fitting to constrain the parameters of the phase-type distributions in the reduced model (section 2.4).

4.1. Partitioning schemes

Aggregating full model states according to the number of open channels leads to a block tridiagonal matrix with skip-free transitions between blocks. Consequently, the phase-type distributions for the interior blocks $1 \leq i \leq N - 1$ have two starting distributions (α^\pm) and two exit vectors (u^\pm) in both the homogenized full model and the reduced model.

While it is important to choose a partition structure that does not combine full model states that correspond to different N_O , it is not required to combine full model states that correspond to a given N_O into a single aggregate class. If a large block contributes substantially to the reduction error, the partition can be refined to subdivide this block (e.g., into components with lesser or greater numbers of refractory channels). Such partitioning may be useful when the refractory channels play a complex dynamic role in spark termination as in figure 1(b). Of course, when multiple diagonal blocks correspond to the same N_O , the homogenized full model is no longer tridiagonal (cf (15)).

In the general case, a partitioning scheme will result in n_α ways to enter and n_u ways to leave a given block. Associated with this block are n_α phase-type distributions, each involving a transient matrix T , n_u exit vectors, and one of the n_α initial distributions.

4.2. Moment fitting

The moment fitting procedures that are appropriate to constrain parameters of the reduced model depend on the chosen partition structure, the block size used in the reduced model, and the class of phase-type distribution used in the reduced model. While moment-fitting techniques exist to fit arbitrary phase-type distributions [55, 56], we use two-state hyper-exponential distributions in the reduced model because this results in a tractable moment fitting problem (section 2.4). If the block size used in the reduced model were larger than 2, a direct extension of the approach used here would require further analysis. A less direct extension that bypasses this analytical work and emphasizes more sophisticated non-linear optimization strategies might be preferable. If the hyper-exponential distributions of section 2.4 were extended to n -states, the parameters α^\pm and u^\pm imply $2(n-1)+2n = 4n-2$ degrees of freedom (in this paper $n = 2$ and there are six free parameters). Fitting $k+1$ joint moments m_0^\pm, \dots, m_k^\pm leads to $2(k+1)$ equations. Provided $2(k+1) \geq 4n-2$, the moment fitting will be well-defined, though perhaps overconstrained. On the other hand, the accuracy of the moment fitting step in the model reduction process ($< 10^{-3}$) suggests that such

extensions are not required (figure 7, broken lines). An obvious avenue for further research is exploration of alternative partition structures and the resulting tradeoff between the reduction error and the size of the reduced model.

4.3. Validation to experimental observations

While the three-state model (1) was chosen for illustrative simplicity rather than biophysical realism, it is informative to see if the full (and more importantly reduced) model can reproduce some recent experimental observations. For example, in [50] measurements using total internal reflection fluorescence microscopy were able to capture the quantal structure of calcium release from clusters of IP_3R channels in mammalian cells. Subsequent analysis showed that for closing events that showed no channel openings during the falling phase, the histogram of puff durations (more specifically time from peak amplitude to closure, scaled by the mean blip duration) was well approximated by a distribution corresponding to the closing time for a representative number of stochastic and independent channels, each closing with time constant given by the mean blip duration. The same analysis applied to simulations of the full three-state model (1) showed similar results (not shown). More importantly, the results were nearly identical for the reduced model as well.

It was posited in [50] that this close approximation may be due to the strong Ca^{2+} -dependent inhibition seen in type I IP_3R channels. Surprisingly, this agreement of the closure of stochastic and independent channels with simulated events was seen for both parameter sets corresponding to closure via the gradual recruitment of inactivated channels and via stochastic attrition.

4.4. Ca^{2+} release site reduction and multiscale modeling

The reduction strategy presented and validated here is an important step toward the goal of including realistic compositional release site models in multiscale whole cell simulations (see section 1). With this objective in mind, an avenue for future research is the extension of this reduction technique to Ca^{2+} release site models that take the form

$$Q([\text{Ca}^{2+}]) = K_- + [\text{Ca}^{2+}]K_+,$$

where $[\text{Ca}^{2+}](t)$ is an external ‘environmental’ variable, as opposed to an intrinsic variable that is an instantaneous function of release site state (cf (8)). This could be accomplished by performing model reduction for a number of physiologically realistic Ca^{2+} concentrations and interpolating the rate constants so that, e.g., $Q([\text{Ca}^{2+}]) = \epsilon Q(c_i) + (1 - \epsilon)Q(c_j)$ where $c_i \leq [\text{Ca}^{2+}] \leq c_j$ and $\epsilon = (c_j - [\text{Ca}^{2+}]) / (c_j - c_i)$. A more interesting approach would be to assume that the free parameters of the phase-type distributions of the reduced model ($\hat{\alpha}^\pm, \hat{u}_1^\pm, \hat{u}_2^\pm$) can be written as simple functions of $[\text{Ca}^{2+}]$ (e.g. polynomials of specified degree). The challenge of this approach would be to generalize (18) and develop moment fitting techniques that constrain the coefficients of these polynomial functions of $[\text{Ca}^{2+}]$.

Acknowledgments

This research was supported in part by the National Science Foundation under grant no 0443843 to GDS and a Howard Hughes Medical Institute grant through the Undergraduate Biological Sciences Education Program to The College of William and Mary. This work was performed in part using computational facilities provided with the assistance of the National Science Foundation, the Virginia Port Authority, Sun Microsystems, and Virginia's Commonwealth Technology Research Fund.

Appendix. Moment-fitting for first and last blocks

The scheme employed to fit the moments of the two-state hyper-exponential distributions in the reduced model to the moments calculated from the interior blocks of the full model T_i for $1 \leq i \leq N-1$ are modified when $i = 0$ or N . The reduction of the block row corresponding to $N_O = N$ is not required, because the full model has only one state in this group (all channels in state \mathcal{O}) and $T_N = -u_N^-$ and $\alpha_N^- = 1$ are scalars. The reduction of the block row corresponding to $N_O = 0$ requires a different scheme than the interior blocks because the transient matrix T_0 is associated with one starting distribution (α_0^+) and one exit vector (u_0^+). Dropping the superscript and subscript for clarity and using (17) and (18) we have

$$m_1 = \frac{\hat{\alpha}}{\hat{u}_1} + \frac{1 - \hat{\alpha}}{\hat{u}_2}$$

$$m_2 = 2 \left(\frac{\hat{\alpha}}{\hat{u}_1^2} + \frac{1 - \hat{\alpha}}{\hat{u}_2^2} \right)$$

$$m_3 = 6 \left(\frac{\hat{\alpha}}{\hat{u}_1^3} + \frac{1 - \hat{\alpha}}{\hat{u}_2^3} \right),$$

where we have equated the first three reduced model moments to the target moments of the full model ($\hat{m}_k = m_k$). These expressions are partially inverted to obtain

$$m_1 \hat{u}_1 \hat{u}_2 = \hat{\alpha} \hat{u}_2 + (1 - \hat{\alpha}) \hat{u}_1$$

$$m_2 \hat{u}_1^2 \hat{u}_2^2 = 2 \hat{\alpha} \hat{u}_2^2 + 2(1 - \hat{\alpha}) \hat{u}_1^2$$

$$m_3 \hat{u}_1^3 \hat{u}_2^3 = 6 \hat{\alpha} \hat{u}_2^3 + 6(1 - \hat{\alpha}) \hat{u}_1^3.$$

After some algebra, we write $x = \hat{u}_1 + \hat{u}_2$ and $y = \hat{u}_1 \hat{u}_2$ and simultaneously solve

$$0 = 2m_1 x - m_2 y - 2$$

$$0 = m_3 y^2 - 6m_1(x^2 - y) + 6x.$$

We let x be the larger of the two solutions to the following quadratic equation:

$$(2m_3 m_1^2 - 3m_1 m_2^2)x^2 + (6m_1^2 m_2 + 3m_2^2 - 4m_1 m_3)x + 2m_3 - 6m_1 m_2 = 0$$

and y is given by

$$y = \frac{2(m_1 x - 1)}{m_2}.$$

Finally, the parameters of the hyper-exponential distribution are given by

$$\alpha = \frac{\hat{u}_1(m_1 \hat{u}_2 - 1)}{\hat{u}_2 - \hat{u}_1} \quad \text{and} \quad \hat{u}_{1/2} = \frac{x \pm \sqrt{x^2 - 4y}}{2}.$$

References

- [1] Bray D 1998 Signaling complexes: biophysical constraints on intracellular communication *Annu. Rev. Biophys. Biomol. Struct.* **27** 59–75
- [2] Gomperts B D, Tatham P E R and Kramer I M 2002 *Signal Transduct.* (New York: Academic)
- [3] Duke T A and Bray D 1999 Heightened sensitivity of a lattice of membrane receptors *Proc. Natl Acad. Sci. USA* **96** 10104–8
- [4] Goldstein B, Faeder J R, Hlavacek W S, Blinov M L, Redondo A and Wofsy C 2002 Modeling the early signaling events mediated by FcεR1 *Mol. Immunol.* **38** 1213–9
- [5] Wilson B S, Pfeiffer J R, Smith A J, Oliver J M, Oberdorf J A and Wojcikiewicz R J 1998 Ca²⁺-dependent clustering of inositol 1,4,5-trisphosphate receptors *Mol. Biol. Cell* **9** 1465–78
- [6] Berridge M J 1997 Elementary and global aspects of Ca²⁺ signalling *J. Physiol.* **499** 291–306
- [7] Cho W 2006 Building signaling complexes at the membrane *Sci. STKE* **2006** pe7
- [8] Berridge M J 2006 Calcium microdomains: organization and function *Cell Calcium* **40** 405–12
- [9] Yao Y, Choi J and Parker I 1995 Quantal puffs of intracellular Ca²⁺ evoked by inositol trisphosphate in *Xenopus* oocytes *J. Physiol.* **482** 533–53
- [10] Sun X P, Callamaras N, Marchant J S and Parker I 1998 A continuum of IP₃-mediated elementary Ca²⁺ signalling events in *Xenopus* oocytes *J. Physiol.* **509** 67–80
- [11] Mak D O and Foskett J K 1997 Single-channel kinetics, inactivation and spatial distribution of inositol trisphosphate (IP₃) receptors in *Xenopus* oocyte nucleus *J. Gen. Physiol.* **109** 571–87
- [12] Foskett J K, White C, Cheung K H and Mak D O 2007 Inositol trisphosphate receptor Ca²⁺ release channels *Physiol. Rev.* **87** 593–658
- [13] Stern M D, Song L S, Cheng H, Sham J S, Yang H T, Boheler K R and Rios E 1999 Local control models of cardiac excitation–contraction coupling. A possible role for allosteric interactions between ryanodine receptors *J. Gen. Physiol.* **113** 469–89
- [14] Cheng H and Lederer W J 2008 Calcium sparks *Physiol. Rev.* **88** 1491–545
- [15] Swillens S, Dupont G, Combettes L and Champeil P 1999 From Ca²⁺ blips to Ca²⁺ puffs: theoretical analysis of the requirements for interchannel communication *Proc. Natl Acad. Sci. USA* **96** 13750–5
- [16] Nguyen V, Mathias R and Smith G D 2005 A stochastic automata network descriptor for Markov chain models of instantaneously-coupled intracellular Ca²⁺ channels *Bull. Math. Biol.* **67** 393–432
- [17] Groff J R and Smith G D 2008 Ryanodine receptor allosteric coupling and the dynamics of calcium sparks *Biophys. J.* **95** 135–54
- [18] Shuai J W and Jung P 2002 Stochastic properties of Ca²⁺ release of inositol 1,4,5-trisphosphate receptor clusters *Biophys. J.* **83** 87–97
- [19] Falcke M 2003 On the role of stochastic channel behavior in intracellular Ca²⁺ dynamics *Biophys. J.* **84** 42–56
- [20] Shuai J W and Jung P 2003 Optimal ion channel clustering for intracellular calcium signaling *Proc. Natl Acad. Sci. USA* **100** 506–10
- [21] Thul R and Falcke M 2006 Frequency of elemental events of intracellular Ca²⁺ dynamics *Phys. Rev. E* **73** 061923
- [22] Skupin A, Kettenmann H and Falcke M 2010 Calcium signals driven by single channel noise *PLoS Comput. Biol.* **6** e1000870
- [23] DeRemigio H, Kemper P, LaMar M D and Smith G D 2008 Markov chain models of coupled intracellular calcium

- channels: Kronecker structured representations and benchmark stationary distribution calculations *Phys. Biol.* **5** 36003
- [24] Hao Y, Kemper P and Smith G D 2009 Reduction of calcium release site models via fast/slow analysis and iterative aggregation/disaggregation *Chaos (Focus issue: Intracellular Calcium Dynamics—A Change of Modeling Paradigm?)* **19** 037107
- [25] Colquhoun D and Hawkes A G 1995 A Q -matrix cookbook: how to write only one program to calculate the single-channel and macroscopic predictions for any kinetic mechanism *Single-Channel Recording* ed B Sakmann and E Neher (New York: Plenum) pp 589–633
- [26] Smith G D 2002 Modeling the stochastic gating of ion channels *Computational Cell Biology* ed C P Fall, E S Marland, J M Wagner and J J Tyson (Berlin: Springer) pp 291–325
- [27] Groff J R, DeRemigio H and Smith G D 2010 Markov chain models of ion channels and the collective gating of Ca^{2+} release sites *Stochastic Methods in Neuroscience* ed C Laing and L Gabriel (Oxford: Oxford University Press) pp 29–64
- [28] De Young G W and Keizer J 1992 A single-pool inositol 1,4,5-trisphosphate-receptor-based model for agonist-stimulated oscillations in Ca^{2+} concentration *Proc. Natl Acad. Sci. USA* **89** 9895–9
- [29] Keizer J and Levine L 1996 Ryanodine receptor adaptation and Ca^{2+} -induced Ca^{2+} release-dependent Ca^{2+} oscillations *Biophys. J.* **71** 3477–87
- [30] Sneyd J, Falcke M, Dufour J F and Fox C 2004 A comparison of three models of the inositol trisphosphate receptor *Prog. Biophys. Mol. Biol.* **85** 121–40
- [31] Norris J R 1997 *Markov Chains* (Cambridge: Cambridge University Press)
- [32] Stewart W J 1994 *Introduction to the Numerical Solution of Markov Chains* (Princeton, NJ: Princeton University Press)
- [33] Ríos E and Stern M D 1997 Calcium in close quarters: microdomain feedback in excitation–contraction coupling and other cell biological phenomena *Annu. Rev. Biophys. Biomol. Struct.* **26** 47–82
- [34] Swillens S, Champeil P, Combettes L and Dupont G 1998 Stochastic simulation of a single inositol 1,4,5-trisphosphate-sensitive Ca^{2+} channel reveals repetitive openings during ‘blip-like’ Ca^{2+} transients *Cell Calcium* **23** 291–302
- [35] Smith G D, Dai L, Muira R and Sherman A 2001 Asymptotic analysis of equations for the buffered diffusion of intracellular Ca^{2+} *SIAM J. Appl. Math.* **61** 1816–38
- [36] Naraghi M and Neher E 1997 Linearized buffered Ca^{2+} diffusion in microdomains and its implications for calculation of $[\text{Ca}^{2+}]$ at the mouth of a Ca^{2+} channel *J. Neurosci.* **17** 6961–73
- [37] DeRemigio H and Smith G D 2005 The dynamics of stochastic attrition viewed as an absorption time on a terminating Markov chain *Cell Calcium* **38** 73–86
- [38] DeRemigio H and Smith G D 2008 Calcium release site ultrastructure and the dynamics of puffs and sparks *Math. Med. Biol.* **25** 65–85
- [39] Groff J R and Smith G D 2008 Calcium-dependent inactivation and the dynamics of calcium puffs and sparks *J. Theor. Biol.* **253** 483–99
- [40] Williams G S B, Huertas M A, Sobie E A, Jafri M S and Smith G D 2007 A probability density approach to modeling local control of Ca^{2+} -induced Ca^{2+} release in cardiac myocytes *Biophys. J.* **92** 2311–28
- [41] Williams G S B, Huertas M A, Sobie E A, Jafri M S and Smith G D 2008 Moment closure for local control models of Ca^{2+} -induced Ca^{2+} release in cardiac myocytes *Biophys. J.* **95** 1689–703
- [42] Huertas M A, Smith G D and Györke S 2010 Analysis of calcium alternans in a cardiac myocyte model that uses moment equations to represent heterogenous junctional SR calcium *Biophys. J.* **99** 377–87
- [43] Skupin A and Falcke M 2009 From puffs to global Ca^{2+} signals: how molecular properties shape global signals *Chaos* **19** 037111
- [44] Winslow R L, Tanskanen A, Chen M and Greenstein J L 2006 Multiscale modeling of calcium signaling in the cardiac dyad *Ann. New York Acad. Sci.* **1080** 362–75
- [45] Derisavi S, Kemper P and Sanders W H 2004 Symbolic state-space exploration and numerical analysis of state-sharing composed models *Linear Algebr. Appl.* **386** 137–66
- [46] Derisavi S, Kemper P and Sanders W H 2005 Lumping matrix diagram representations of Markov models *2005 Int. Conf. on Dependable Systems and Networks* (Los Alamitos, CA: IEEE Computer Society Press) pp 742–51
- [47] Quinn M Mc, Kemper P and Sanders W H 2007 Dependability analysis with Markov chains—how symmetries improve symbolic computations *Int. Conf. on Quantitative Evaluation of Systems (QEST)* ed M Harchol-Balter, M Kwiatkowska and M Telek (Los Alamitos, CA: IEEE Computer Society Press) pp 151–60
- [48] Koury J, McAllister D and Stewart W 1984 Iterative methods for computing stationary distributions of nearly completely decomposable Markov chains *SIAM J. Algebr. Discrete Methods* **5** 164–86
- [49] Cao W L and Stewart W 1985 Iterative aggregation/disaggregation techniques for nearly uncoupled Markov chains *J. Assoc. Comput. Mach.* **32** 702–19
- [50] Smith I F and Parker I 2009 Imaging the quantal substructure of single IP_3R channel activity during Ca^{2+} puffs in intact mammalian cells *Proc. Natl Acad. Sci. USA* **106** 6404–9
- [51] Keener J 2009 Invariant manifold reductions for Markovian ion channel dynamics *J. Math. Biol.* **58** 447–57
- [52] Earnshaw B A and Keener J P 2010 Invariant manifolds of binomial-like nonautonomous master equations *SIAM J. Appl. Dyn. Syst.* **9** 568–88
- [53] Buchholz P, Kemper P and Kriege J 2010 Multi-class Markovian arrival processes and their parameter fitting *Perform. Eval.* **67** 1092–106
- [54] Telek M and Heindl A 2003 Matching moments for acyclic discrete and continuous phase-type distributions of second order *Int. J. Simul.* **3** 47–57
- [55] Asmussen S, Nerman O and Olsson M 1996 Fitting phase-type distributions via the EM algorithm *Scand. J. Stat.* **23** 419–41
- [56] Horvath A and Telek M 2002 Phfit: a general phase-type fitting tool *Computer Performance Evaluation: Modelling Techniques and Tools (Lecture Notes in Computer Science vol 2324)* (Berlin: Springer) pp 1–14